nature catalysis

Article

https://doi.org/10.1038/s41929-023-00952-1

Iron-only Fe-nitrogenase underscores common catalytic principles in biological nitrogen fixation

Received: 2 August 2022

Accepted: 28 March 2023

Published online: 27 April 2023

Check for updates

Christian Trncik, Franka Detemple & Oliver Einsle

Nitrogenases uniquely reduce atmospheric N_2 to bioavailable ammonium. They group into three isoforms that primarily differ in the architecture of their active-site cofactors. A molybdenum or vanadium ion is introduced into a common precursor cluster to form Mo- and V-dependent nitrogenases, respectively. In contrast, the third class of the enzyme only utilizes abundant iron to reduce N_2 under ambient conditions and is consequently of high interest for mechanistic studies and catalyst design. Here we report the three-dimensional structure of Fe-nitrogenase from *Azotobacter vinelandii* and its FeFe cofactor, a [8Fe:9S:C] cluster with an interstitial carbide and an organic homocitrate ligand at the apical iron that substitutes for Mo or V in the other isoforms. The structure reveals lability of sulfide S2B, the proposed binding site for substrate in other nitrogenases, further supporting a general mechanism of proton and electron transfer for all nitrogenases and all their substrates.

Nitrogen is an essential part of all classes of biological macromolecules and therefore an indispensable nutrient for all organisms. Because of the extraordinary chemical stability of the N_2 molecule, it represents a sink for more than 99% of all nitrogen cycling through Earth's biosphere[1], and its assimilation into biomass is only possible through activated forms, in particular ammonium, NH_4^+ (ref. 2). The reductive conversion of N_2 is achieved through atmospheric lightning discharge, the industrial Haber–Bosch process or through biological nitrogen fixation by the enzyme nitrogenase[3]. Industrial N_2 fixation utilizes an iron catalyst at high temperature and pressure (250 bar, 450 °C) to react a syngas N_2/H_2 mixture to ammonia, which is then further processed into suitable fertilizers such as ammonium nitrate[4], with H_2 serving both as a reductant and a proton source for ammonia formation. This is of ecological concern, as presently H_2 is predominantly obtained through steam reforming of natural gas (equation (1)):

$$CH_4 + H_2O \Leftrightarrow 3\,H_2 + CO \quad (1)$$

which requires substantial energy and releases CO and CO_2 as side products. Fertilizer synthesis via the Haber–Bosch process consumes ~2% of the world energy production and releases the equivalent of almost two tonnes of CO_2 per tonne of N_2 (ref. 5). The global production of nitrogen for fertilizers equals the sum of all biologically fixed N_2, and more than half of the current human population depends on food grown on fertilized soil[1]. Several strategies are being followed to mitigate the dependency on nitrogen fertilizers, rooted in the fact that biological nitrogen fixation is limited to diazotrophic microorganisms and is absent in eukaryotes. Efforts are under way to engineer food crops to recombinantly produce an active nitrogenase that would allow them to independently meet their nitrogen requirements[6]. The heterologous production of nitrogenase, however, is a highly complex process, as has been reviewed extensively elsewhere[7,8]. Although the reaction of nitrogenase is indispensable for sustaining organismic growth on Earth, evolution has only produced a single type of enzyme able to break the N_2 triple bond and provide bioavailable ammonium. Nitrogenase is a large enzyme system consisting of two component proteins that dynamically form and break a complex during the six-electron reduction of N_2 to two NH_4^+. Catalysis takes place at a dinitrogenase component, while a dinitrogenase reductase delivers the required electrons and is also the site of adenosine triphosphate (ATP) hydrolysis to drive the reaction[9,10]. The homodimeric reductase is termed the Fe protein, as it contains a [4Fe:4S] cluster at its interface. The three known isoforms of

Institute for Biochemistry, University of Freiburg, Freiburg, Germany. e-mail: einsle@biochemie.uni-freiburg.de

https://doi.org/10.1038/s41929-023-00952-1

dinitrogenases differ in their catalytic properties and in the heterometal ion incorporated into their active site. All known diazotrophs possess a Mo-nitrogenase with a [Mo:7Fe:9S:C]:homocitrate cluster, the FeMo cofactor[11–14]. Some organisms additionally contain a second enzyme dependent on vanadium, with a [V:7Fe:8S:C:CO_3]:homocitrate cluster, the FeV cofactor[15]. The third class of the enzyme, Fe-only nitrogenase, does not require any further heterometal beside iron, but its architecture and cofactor structure have remained unknown so far. According to their class, the dinitrogenases are called *M*Fe proteins (*M* = Mo, V, Fe). Their N_2-reducing activity decreases from MoFe, to VFe and to the FeFe protein, and the latter two are therefore often considered backup systems[9]. However, the simpler cluster architecture of the FeFe protein has allowed recombinant production of Fe-only nitrogenase from *Klebsiella oxytoca* in a heterologous host[16]. This required a total of only ten gene products, and its exclusive dependence on highly available iron and a less complex assembly pathway makes Fe-only nitrogenase a prime target for refactoring the ability for diazotrophic growth in a heterologous host (aiming for eukaryotes and eventually food crops), thus alleviating the dependency on inorganic fertilizers[17,18]. Alternative nitrogenases also show differential reactivities beyond the scope of the canonical substrates of this enzyme. V-dependent nitrogenase, and to a lesser extent the Fe-only isoenzyme, reduce CO to hydrocarbons in analogy to the industrial Fischer–Tropsch process[19], albeit with far lower activity than for N_2. Furthermore, for Fe-nitrogenase, a very low reactivity towards CO_2 was reported that, judging by the growth of a co-cultured methylotroph[20] and by subsequent in vitro studies, leads to methane (CH_4) as the main product[21,22]. Nitrogenase enzymes are thus considered to be prime targets for biotechnological applications, but the mechanistic details of their differential catalytic properties remain to be understood.

After devising a strategy for producing V-nitrogenase by molybdenum depletion during growth of the model diazotroph *Azotobacter vinelandii*[23], we further depleted the growth medium of vanadate and established the induction of Fe-only nitrogenase and its efficient isolation by chromatographic methods[24]. FeFe protein was crystallized, and here we report its three-dimensional (3D) structure at high resolution, the architecture of its metal clusters and a comparison with the other classes of nitrogenases. We conclude that a repetitive sequence of basic elementary steps at the cofactor explains the known aspects of nitrogenase catalysis, in agreement with multiple lines of experimental evidence.

Results

Architecture of the FeFe protein

FeFe protein was isolated from *A. vinelandii* DJ[25] cells that were depleted of the heterometals Mo and V over several cycles of growth, leading to the exclusive production of the Fe-only nitrogenase. Both component proteins were isolated by chromatographic methods (Extended Data Fig. 1). The 3D structure of the Fe protein AnfH is reported elsewhere[24]. The FeFe protein crystallized in the orthorhombic space group $P2_12_12_1$, with one $AnfD_2K_2G_2$ heterohexamer in the asymmetric unit. Diffraction data from these crystals were anisotropic and could be recorded to better than 1.6 Å resolution along *a*, but only to 2.6 Å along *b* and 2.3 Å along *c*. The phase problem was solved by molecular replacement. FeFe protein forms a *C*2-symmetric assembly similar to MoFe protein and VFe protein (Fig. 1a). The core of all three nitrogenases is the D_2K_2 heterotetramer that in VFe protein and FeFe protein is complemented by an additional subunit, VnfG or AnfG, respectively. The G subunits are in exclusive contact with the D subunits and do not contain any metal clusters. Their assumed function is in cofactor delivery for the correct maturation of these dinitrogenases (Fig. 1b)[26]. In FeFe protein, the AnfD subunit differs from NifD of the same organism with a root-mean-squared displacement (r.m.s.d.) of 1.14 Å and from VnfD with an r.m.s.d. of 0.66 Å for all atoms. For AnfK, the r.m.s.d. from NifK is 1.30 Å, and from VnfK it is 0.62 Å. The VnfG and AnfG proteins differ,

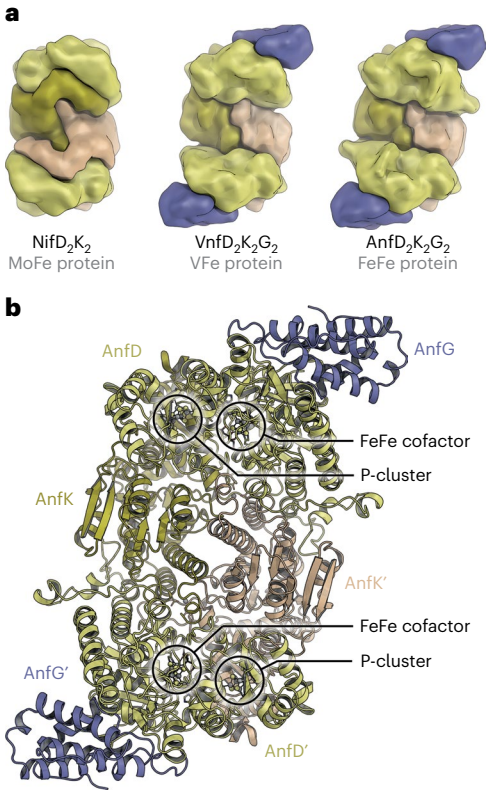

Fig. 1 | Architecture of the FeFe protein of Fe-only nitrogenase. a, Domain architecture of the three isoforms of nitrogenases. D subunits are shown in yellow, K subunits in olive/sand and G subunits in blue. MoFe protein, PDB 3U7Q; VFe protein, PDB 5N6Y. **b**, Cartoon representation of the FeFe protein. Despite differences such as the extended C termini of AnfD, the overall structure of all dinitrogenases is highly similar. The P-clusters are located on the pseudo-two-fold axis relating AnfD and AnfK, and the FeFe cofactor is cradled between the three Rossmann-fold domains of AnfD.

with an r.m.s.d. of 0.82 Å. As indicated by their respective amino-acid sequence similarities, the VFe protein and FeFe protein are structurally more similar than either is with the MoFe protein (Extended Data Fig. 2). The apparent difference in appearance of the three isoenzymes is partly due to the D_2K_2 interface, which is free in the VFe protein, but is covered by the N terminus of NifK in the MoFe protein, and by the C terminus of AnfD in the FeFe protein (Extended Data Fig. 3). All three enzymes contain an electron-transferring P-cluster located on the pseudo-two-fold axis relating the AnfD and AnfK subunits, and the active-site FeFe cofactor is cradled between the three Rossmann-type βαβ domains of the AnfD subunit (Fig. 1b). The identity of the metal sites in the two clusters of the protein was confirmed by anomalous double-difference maps calculated from two diffraction datasets around the X-ray absorption K-edge of Fe (7,120 eV). In the electron density maps, the [8Fe:7S] P-cluster was modelled in its all-ferrous P^N state (Fig. 2a and Extended Data Fig. 4). Functionally, P-clusters reside in the P^N state until the binding of reduced and ATP-loaded Fe protein (here AnfH) to the AnfD–AnfK interface triggers ATP hydrolysis in the reductase and the transfer of an electron from the P-cluster to the active-site FeFe cofactor. Only then is the P-cluster reduced back to the P^N state from the [4Fe:4S] cluster of AnfH[27–29].

Catalytic FeFe cofactor

The second metal cluster of the FeFe protein is the FeFe cofactor, the active site of substrate reduction, and the high-resolution electron density map of the FeFe protein in conjunction with anomalous double difference maps allowed for an unambiguous assignment and modelling of its atomic structure (Fig. 2b). The FeFe cofactor is a

https://doi.org/10.1038/s41929-023-00952-1

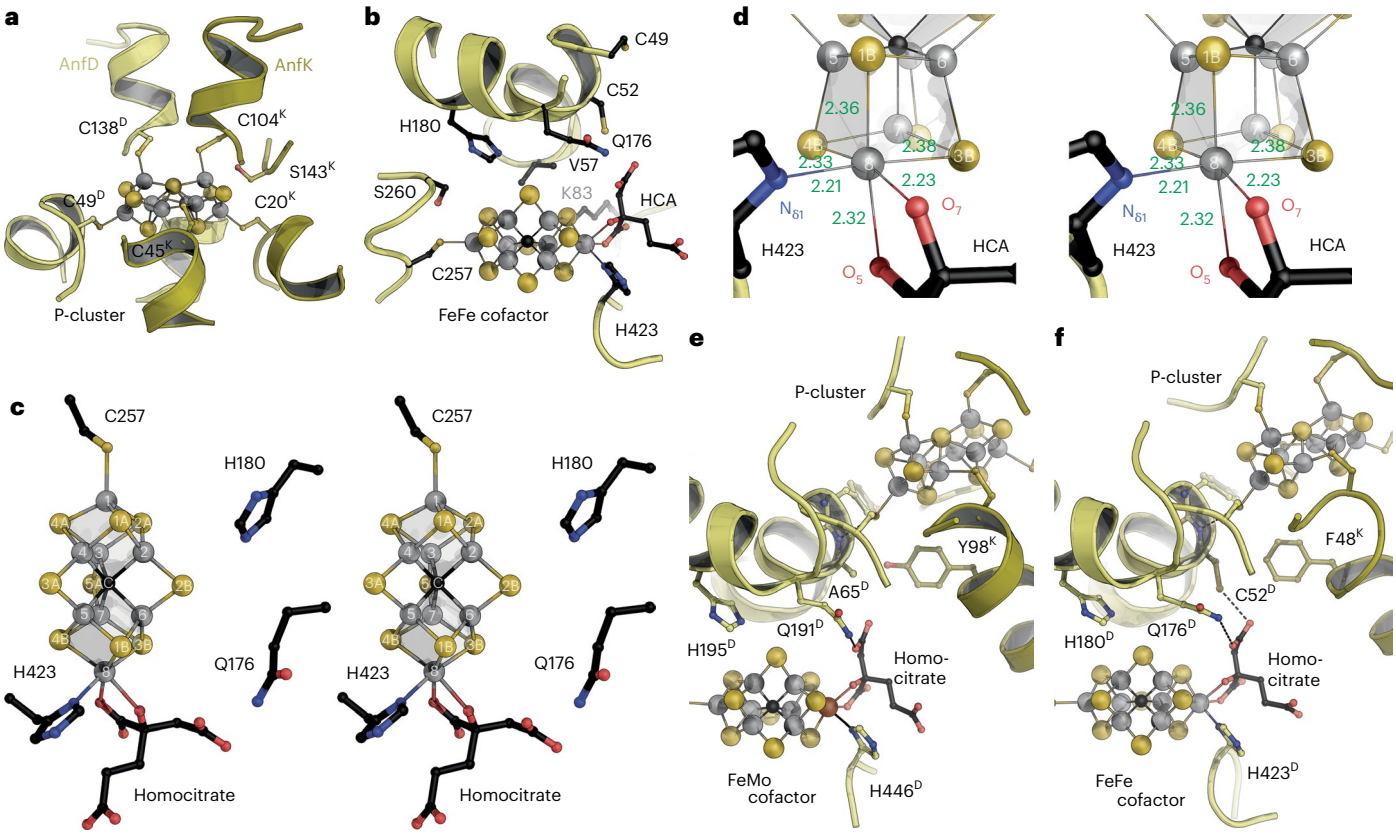

Fig. 2 | The metal clusters of FeFe protein. a, The P-cluster is observed predominantly in its symmetric, all-ferrous P^N state and is located on the pseudo-two-fold symmetry axis relating subunits AnfD and AnfK. **b**, The FeFe cofactor is embedded in the AnfD subunit and coordinated by $C257^D$ to Fe1 and $His423^D$ to Fe8. **c**, Stereo representation of the FeFe cofactor, a D32-symmetric [8Fe:9S:C] cluster that carries an organic homocitrate ligand. The atoms of the cofactor are labelled in accordance with the standard for FeMo and FeV cofactor. **d**, Stereo representation of the ligand environment of Fe8 in the FeFe cofactor. Bond distances (in ångstrom) represent the average of the two copies of the cofactor in the FeFe protein structure. **e**, Electron-transfer pathway between the P-cluster and FeMo cofactor in *A. vinelandii* MoFe protein (PDB 3U7Q) with the conserved $Tyr98^K$. **f**, The region between the FeFe cofactor and the P-cluster in FeFe protein. The tyrosine is replaced by $Phe48^K$, but residue $Cys52^D$ can instead provide a hydrogen bond to the homocitrate moiety of the cofactor.

[8Fe:9S:C]:homocitrate cluster that shows *D*32 symmetry in its inorganic part and contains a central carbide as an interstitial ligand of a trigonal prism formed by iron ions Fe2–Fe7 (Fig. 2c)[30]. This rigid prism, reminiscent of carbon-doped steel[31], is a hallmark of nitrogenase cofactors and is capped by irons Fe1 and Fe8, with the latter taking the place of Mo or V in the respective isoforms of nitrogenase. Fe1 is ligated by residue $Cys257^D$, and Fe8 is coordinated by homocitrate and by residue $His423^D$. The bond distances around Fe8 match those in the other nitrogenases, with the Fe–N and Fe–O bonds being slightly shorter than those in the heavier heterometals (Fig. 2d). In the immediate surroundings, $His180^D$ and $Gln176^D$ attain the same positions as in the other classes of nitrogenases, well in line with the suggested mechanistic relevance of these residues[9,32,33] and a common mechanism of N_2 reduction for all nitrogenases[34]. The FeFe cofactor can be interpreted as two symmetric half-cubanes fused via the interstitial carbide and, as in the FeMo cofactor, bridged by three μ_2-sulfides, S2B (Fe2 and Fe6), S3A (Fe4 and Fe5) and S5A (Fe3 and Fe7; Fig. 2c).

Intramolecular electron transfer

The closest distance between the P-cluster and cofactor within the FeFe protein is 14 Å, but amino-acid residues and water molecules were previously implicated in their communication. $Tyr98^K$ of the MoFe protein was suggested to support electron transfer[35], and its exchange for histidine had enabled the MoFe protein to reduce hydrazine (N_2H_4) without requiring Fe protein or ATP, but not the inert N_2 molecule (Fig. 2e)[36]. In the FeFe protein, the amino acid corresponding to the Tyr98 of NifK is the Phe48 of AnfK, which is still aromatic, but seems less well suited to promote electron transfer as it cannot support a hydrogen-bonding network (Fig. 2f). However, the AnfD subunit contains a cysteine at position 52 that is absent in NifD ($Ala65^D$) and that may substitute for Tyr in the FeFe protein. The V-nitrogenase of *A. vinelandii* also contains this Phe–Cys combination and lacks a tyrosine in this region. $Cys52^D$ is in direct hydrogen-bonding contact with the homocitrate ligand to the active-site FeFe cofactor (Fig. 2b). Although the V- and Fe-nitrogenases of *A. vinelandii* feature the Phe–Cys pair, all available structures of the Mo-dependent isoenzyme from *A. vinelandii*, *Clostridium pasteurianum*[37], *Klebsiella pneumoniae*[38] and *Gluconacetobacter diazotrophicus*[39] show the Tyr–Ala set-up. The organic homocitrate ligand is formed from 2-oxoglutarate and acetyl-coenzyme A by NifV, a canonical *R*-homocitrate synthase (Extended Data Fig. 5)[40]. Its action is required for all three nitrogenases[41], and it is also essential for the recombinant production of Fe-nitrogenase in *Escherichia coli*[16].

Resting and turnover states

The FeFe cofactor shares key features of the previously characterized FeMo and FeV cofactors, including a similar degree of intrinsic structural flexibility. This was first observed when MoFe protein was turned over in the presence of CO, a non-competitive inhibitor for the reduction of all substrates other than protons[42], leading to the replacement of sulfide S2B with CO as a carbonyl bridging Fe2 and Fe6[43]. In a subsequent study, the reduction of SeCN by Mo-nitrogenase again resulted in the replacement of S2B, and under continuous turnover also to a lesser

https://doi.org/10.1038/s41929-023-00952-1

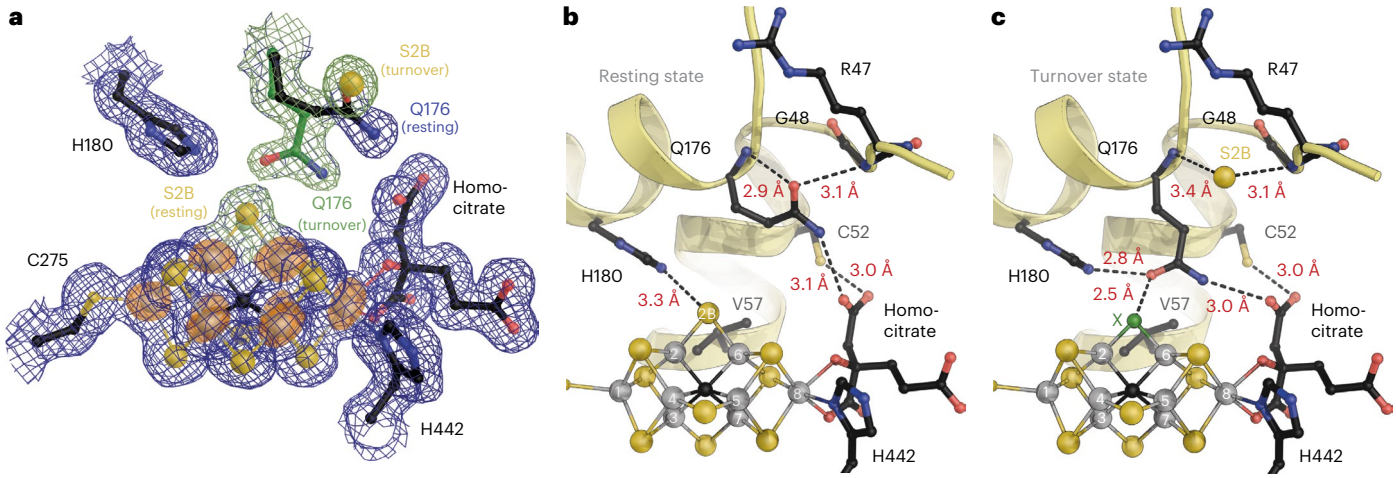

Fig. 3 | Conformations of FeFe cofactor. a, Electron density features around the FeFe cofactor. The $2F_o–F_c$ electron density map contoured at the 1σ level shows a dual conformation at residue Gln176 due to an equilibrium of a resting (blue) and turnover (green) state, as seen in the structure of V-nitrogenase[33]. An anomalous difference electron density map contoured at the 5σ level from data collected at the Fe K-edge (7,120 eV) highlights the positions of the eight Fe ions of the cofactor. **b**, In the resting-state conformation, Fe2 and Fe6 are bridged by sulfide S2B, and Gln176 points towards a holding site, with its amide nitrogen hydrogen-bonded to the homocitrate ligand to Fe8. **c**, The transition to the turnover state involves the release of sulfide S2B, which migrates to the holding site, displacing the side chain of Gln176, which rotates to form a hydrogen bond to His180. The dinuclear binding site at the Fe2–Fe6 edge is occupied by a light atom (X). The FeFe cofactor thus shows the same functionality as observed for the FeV cofactor.

extent S3A and S5A with Se, indicating substantial structural flexibility of the μ_2-sulfides of the cofactor[44]. After an initial characterization of the resting state[15], the VFe protein of vanadium nitrogenase was then depicted in a turnover state at atomic resolution, where exclusively sulfide S2B was replaced by a light atom that was suggested to represent a reaction intermediate[33]. S2B had in turn migrated to a holding site ~7 Å away from the cluster, which triggered the rearrangement of the side chain of the conserved $Gln176^D$. In its new position, $Gln176^D$ formed a short (2.8 Å) hydrogen bond to residue $His180^D$ and was situated directly above the bound light atom at only 2.55-Å distance[33]. For the FeFe protein, the $F_o–F_c$ difference electron density map now revealed a double conformation for residue $Gln176^D$ that is explained by two alternative conformations for a resting and turnover state of the cofactor (Fig. 3a). In the resting-state conformation, $Gln176^D$ points away from sulfide S2B, with its amide $N_{\varepsilon 2}$ weakly hydrogen-bonding to the α-carboxylate of the homocitrate ligand. The amide $O_{\varepsilon 1}$ simultaneously occupies a cavity, where it forms hydrogen bonds to its own backbone amide and to the one of $Gly48^D$ (Fig. 3b). In a second conformation of the same crystal, residue $Gln176^D$ has rotated its side chain to accept a hydrogen bond from the $N_{\varepsilon 2}$ atom of the imidazole side chain of $His180^D$ to its $O_{\varepsilon 1}$ atom, while retaining its interaction with homocitrate. This requires sulfide S2B to be exchanged for a light atom with shorter bond distances within the cluster, leading to the turnover state[33]. In it, the displaced sulfide (likely as HS^-) relocated to the cavity previously occupied by the $O_{\varepsilon 1}$ atom of $Gln176^D$. In the present $2F_o–F_c$ electron density map, the density peak in this cavity was far stronger than the one for the adjacent $N_{\varepsilon 2}$ atom, confirming the presence of a partially occupied sulfide. The FeFe protein thus crystallized as a mixture of a resting and a turnover state, with an undefined light atom replacing S2B in the latter (Fig. 3c), in fully analogy to our analysis of the FeV cofactor[9,33].

Mechanistic implications

We have argued that the turnover state of the VFe protein helped to rationalize a series of experimental observations in the context of a mechanistic model[32]. The functional and structural similarities of all the nitrogenase cofactors now suggest a common mode of reductive catalysis, and a molecular mechanism for dinitrogenase is taking shape. Nitrogenases facilitate the six-electron reduction of N_2 to $2NH_4^+$, and, in addition, all three isoforms of the enzyme produce H_2 in an undesired side reaction that is more prominent in V- and Fe-only enzymes than in the Mo-dependent one[9]. However, discounting this side reaction, all classes converge towards a minimal stoichiometry for catalytic dinitrogen reduction (equation (2)):

$$N_2 + 10\,H^+ + 8\,e^- + 16\,ATP \rightarrow 2\,NH_4^+ + H_2 + 16\,[ADP + P_i] \quad (2)$$

The mandatory, stoichiometric release of H_2 is an essential feature of the catalytic mechanism. This was reported early on, and was included into the seminal kinetic scheme by Lowe and Thorneley that remains widely accepted now (Extended Data Fig. 4)[45]. The significance of H_2 release was understood when the formation of surface hydrides was proposed as a general mechanism for electron accumulation at the cofactors[46,47]. It explained how successive reduction steps could occur at constant potential, and the accidental protonation of a surface hydride also rationalized why these stored reducing equivalents were frequently lost, and unwanted H_2 was released as a wasteful side reaction[9]. Only after accumulation of four electrons (that is, in the E_4 state) does the kinetic scheme allow for the binding and activation of N_2. Upon binding, N_2 is exchanged for H_2, but now the origin of H_2 is a reductive elimination from two adjacent hydrides[46,48], representing the only means of generating a two-electron-reduced cofactor that is sufficiently reactive to break the N_2 triple bond[32]. Combined with the turnover-state structures of the VFe and FeFe proteins and the available CO complexes of MoFe[43] and VFe protein[49], the emerging picture is that of a binuclear substrate binding site that opens up at Fe2 and Fe6 after removal of sulfide S2B[32]. This may also be where the first hydride forms as a μ_2-bridging ligand to both iron sites[32], or it might initially bind terminally to Fe6[50]. More recently, structures with two bound CO molecules at the FeMo cofactor[51] and FeV cofactor[50] showed the second ligand binding terminally to Fe6, and a similar chemical nature of the strong-field ligands CO and H^- prompted us to suggest that both sites might be relevant for binding hydrides as well as substrate, with a designated bridging μ-site at Fe2 and Fe6 and a terminal t-site at Fe6[50] (Fig. 4a).

As in VFe protein, the dissociation of S2B opens the dinuclear μ-site for substrate binding, and the t-site at Fe6 represents a first point of contact for all substrates with the cluster. This includes the simplest substrate of nitrogenase, a proton, which is required for the

https://doi.org/10.1038/s41929-023-00952-1

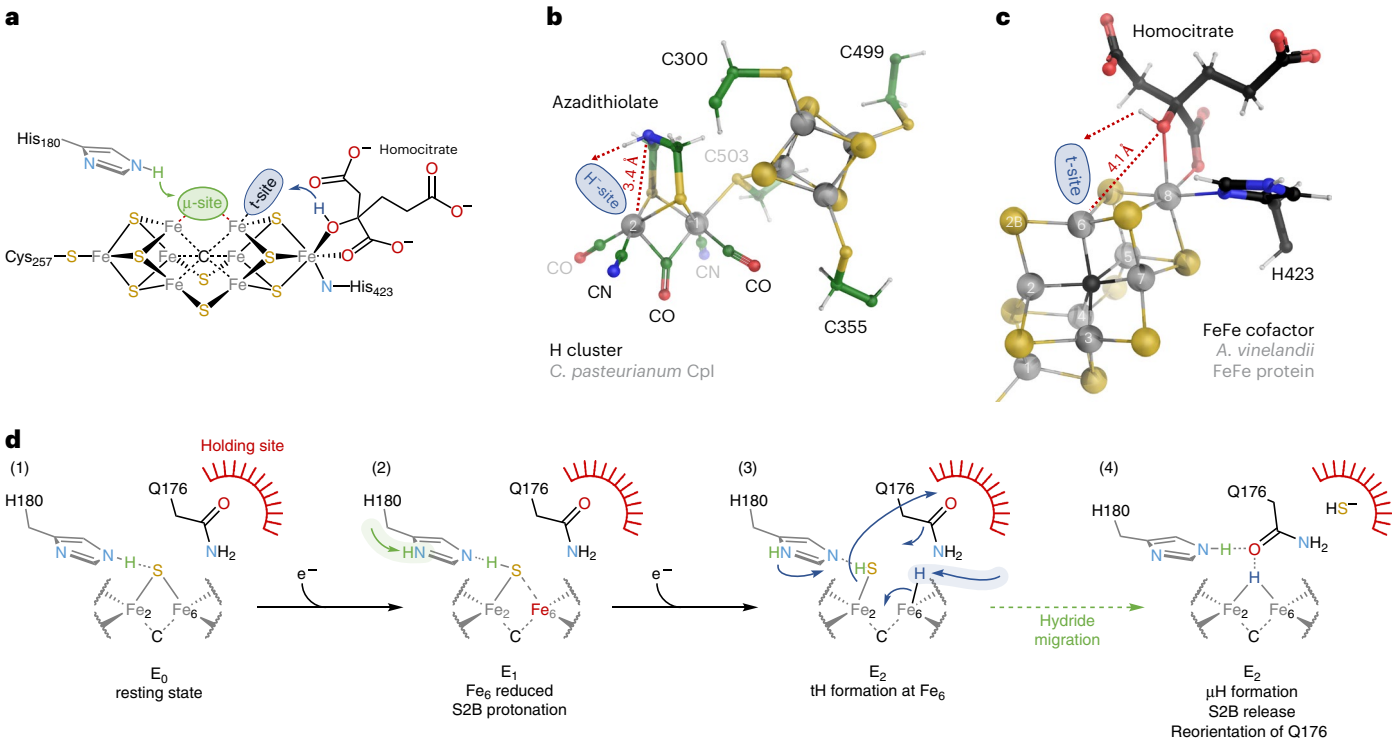

Fig. 4 | Hydride formation and mechanistic implications. a, The 2CO complexes of the MoFe and VFe proteins[51,52] suggested that substrates bind to the Fe2–Fe6 edge, either μ_2-bridging (μ-site) or terminally to Fe6 (t-site). Distinct proton donors supply each position: His180 for the μ-site and the 3′-OH group of homocitrate for the t-site. **b**, In the active-site H cluster of Fe,Fe hydrogenase, an azadithiolate ligand serves as a proton donor to a hydride bound terminally to Fe2 (PDB 1HFE)[62]. **c**, Homocitrate as a proton donor to the t-site presents a similar arrangement, with the 3′-OH group additionally forming an internal hydrogen bond to the α-carboxylate. **d**, Initial activation steps. In resting state E_0, sulfide S2B is in place to coordinate Fe2 and Fe6 and is hydrogen-bonded by $N_{\varepsilon 2}$ of His180 (1). Gln176 points away from the active site and occupies the holding site (red). Electron transfer to E_1 (2) leads to reduction of Fe6, weakening its interaction with S2B, which then receives the proton from His180. This is compensated by a concurrent proton transfer from the medium to the $N_{\delta 1}$ of His180. With the next electron transfer to E_2 (3), a proton is recruited from the 3′-OH group of homocitrate to form a terminal hydride at Fe6. As a key step in nitrogenase catalysis, such terminal hydrides migrate into a bridging position at the Fe2–Fe6 edge, triggering a sequence of events: at Fe2, the dangling sulfhydryl is released as HS^- and migrates to the holding site 7 Å away. In parallel, the proton at $N_{\delta 1}$ of His180 moves to the thermodynamically favoured $N_{\varepsilon 2}$ position, where it can form a hydrogen bond to the γ-amide oxygen of Gln176 that flipped by 180° after being displaced by the free HS^-. The result is a stable E_2 state with a μ_2-hydride at the Fe2–Fe6 edge (4) that is protected from protonation by the presence of Q176 as a hydrogen-bond acceptor from the putative H^+ donor, His180.

formation of a terminal hydride at the t-site once the second electron transfer from the Fe protein promotes the enzyme to the E_2 state. With two distinct binding sites at the Fe2–Fe6 edge, the enzyme also provides two protonation sites, supplying the μ-site from the $His180^D$ above Fe2 and the t-site from the 3′-OH group of homocitrate. However, as nitrogenase must acquire two additional electrons to reach the E_4 state where N_2 activation and subsequent reduction is only possible, the lifetime of the bound hydride in E_2 is critical. If both $His180^D$ and the homocitrate ligand to the FeFe cofactor were available as proton sources, an unwanted hydride loss that would take the system back two steps in its catalytic cycle would be a persistent risk (Extended Data Fig. 6). To prevent this, the rearrangement of $Gln176^D$ that we observe in VFe and FeFe protein serves two purposes. First, reorientation of the glutamine side chain promotes the elimination of S2B as a sulfhydryl anion from the Fe2–Fe6 edge, and by doing so it vacates the holding site for S2B. Second, in its turnover-state conformation, $Gln176^D$ forms a short hydrogen bond to $His180^D$, stabilizing the proton on the $N_{\varepsilon 2}$ atom of the histidine and preventing its release in the proximity of a hydride (Fig. 3c). The t-hydride can now migrate to the open μ-site, where it is bound more tightly. The basic functionality of nitrogenases may then be to iterate through three elementary steps, namely, the reduction of Fe6, the formation of a t-hydride at Fe6 upon the next reduction, with the hydroxyl group of homocitrate as a proton donor, and finally the migration of hydride from the t-site to the μ-site for stability[50]. Further along the catalytic cycle, the t-hydride in the third step would insert into a reaction intermediate already bound at the μ-site, as elaborated elsewhere for the reduction of CO by V-nitrogenase[50]. Crucially, we note that with slow electron transfer and the risk of hydride protonolysis, reaching the E_4 state to activate N_2 is a highly challenging task for the enzyme, while the subsequent reduction of the bound diazene-level intermediate is comparatively facile. A recent proposal of a structure of nitrogenase with two bound N_2 molecules[52] was not only challenged for technical soundness[53,54], but in particular the implied mechanism, also elaborated separately[55], is at variance with most of the tenets of the Lowe–Thorneley scheme and the spectroscopic, structural and theoretical findings referenced here.

Discussion

It is equally surprising that a fundamental metabolic pathway such as the reductive fixation of atmospheric N_2 has evolved only once in the history of life, and that at the same time the nitrogenase enzyme has subsequently diverged into three different isoforms that retain an overall architecture and functionality but utilize a different heterometal at the apex of the catalytic cofactor. As outlined above, all diazotrophs possess a Mo-nitrogenase[56], and phylogenetic analyses indicate this also to be the most ancient form of the enzyme[57]. Why then did the alternative enzymes evolve and persist, despite a lower catalytic activity towards N_2? One possible—yet debated—answer is

that the mentioned activities towards CO (and possibly CO_2) constitute actual secondary metabolic pathways for these organisms[21]. On the other hand, a major factor may be the bioavailability of the heterometal itself. At 10 μg l^{-1}, molybdate is the most abundant transition metal in sea water, where biological nitrogen fixation evolved, but it is orders of magnitude scarcer on land. However, the situation is exactly reversed for the availability of vanadium[21]. The emergence of alternative nitrogenases thus may simply be a tribute to Mo limitation in a new habitat, with the Fe-dependent enzyme as a final fallback. This issue is also more problematic for free-living diazotrophs in cryptogamic covers than for rhizobia, where the deep-reaching plant roots assist in trace metal mobilization. Consequently, alternative nitrogenases become more prevalent at higher latitudes and cold temperatures, where noduled legumes no longer thrive[21].

The structure of an Fe-dependent dinitrogenase completes our knowledge about the architecture of the three isoforms of this enzyme. It corroborates current hypotheses on enzyme function and will help to further integrate spectroscopic and theoretical data. Our work also clarifies the composition and environment of the FeFe cofactor. As a [8Fe:9S:C] moiety in the resting state, the cluster has the symmetric structure proposed earlier based on extended X-ray absorption fine structure studies and on the knowledge of the maturation factors that are involved in its formation. Although all nitrogenase isoforms require the NifB protein to make a common cluster precursor, Fe-nitrogenase does not need an additional component as a scaffold for replacement of the apical metal (NifEN or VnfEN, respectively)[58]. The FeFe cofactor thus derives from the direct product of NifB, the L-cluster or NifB cofactor. Although the apical Fe8 of FeFe cofactor is not exchanged for a heterometal, the cluster carries an organic homocitrate ligand in a conformation that is very similar to those observed for the FeMo and FeV cofactors. Its presence in all three nitrogenases underlines a functional role for homocitrate; its replacement for citrate in a Δ*nifV* strain decreased the enzymatic activity of the resulting MoFe protein substantially[59,60], and, more recently, the protonation of homocitrate has been suggested to be essential for the catalytic reaction[61]. We therefore include homocitrate as a second proton donor into our mechanistic model. Protonation occurs on the 3′-OH group, which is a ligand to the Mo/V/Fe8 in all cofactors and is stabilized by an internal hydrogen bond to the α-carboxylate of the ligand. The arrangement of the elements of this reaction step is reminiscent of the one in [Fe,Fe]-hydrogenase that catalyses the formation of H_2 by protonating a terminal hydride bound to an iron centre[62,63]. Here, the diiron site in the active-site H cluster is bridged by a unique azadithiolene ligand, whose central amide donates a proton (Fig. 4b), with a geometry reminiscent of the positioning of the homocitrate moiety in nitrogenase relative to Fe6 of the cofactor (Fig. 4c).

In the mechanistic interplay of the t-site and the μ-site during catalysis, reduction of the enzyme to an odd-numbered E-state would always trigger proton transfer from the histidine situated above Fe2 (His195 in MoFe, His180 in VFe and FeFe) to the ligand at the μ-site, while the next electron transfer to an even E-state will lead to hydride formation at Fe6, supplied with a proton from homocitrate[50]. Following this principle, the steps leading from the resting state E_0 to a hydride bound to the cofactor in E_2 become readily apparent (Fig. 4d). In the resting state (step 1 in Fig. 4d), His180 provides a 3.3-Å hydrogen bond to sulfide S2B, and Glu176 is directed towards the holding site. The reduction of Fe6 promotes the system to the E_1 state (step 2), which has been previously studied by X-ray absorption spectroscopy[64,65]. Here, the reduction of the metal site weakens the Fe6–S2B bond, leading effectively to the protonation of the sulfide, which is compensated by a proton transfer to the $N_{δ1}$ atom of His180. With the next electron transfer, the resulting E_2 state (step 3) cannot accommodate a two-electron-reduced cofactor, so a surface hydride is formed, initially at the t-site with a proton provided by homocitrate that then migrates to the μ-site or inserts into a bound ligand there. At E_2 there is no such ligand yet, but the hydride migration then triggers an important rearrangement. It displaces the protonated S2B, which leaves the cofactor as HS^- and relocates to the positively charged holding site, causing the less strongly binding Gln176 to rotate away from the holding site and towards the cofactor. Here it forms a short (2.8 Å) hydrogen bond to His180 (step 4), as observed in the turnover-state structures[33], shielding the bound hydride from accidental protonation as detailed above. In the succession of one-electron reductions in the Lowe–Thorneley cycle, electron transfer may consistently terminate at Fe6, and the coupled protonation events will occur alternatingly from homocitrate to the t-site and from the histidine to the μ-site. In the initial charging phase of the cluster (E_1–E_4), this shielding effect is crucial, as electron transfer from the Fe-protein to the dinitrogenase is slow, and the protonation of bound hydrides leads to the observed, unwanted release of H_2. This becomes even more critical as the enzyme proceeds to E_3 and eventually E_4, where a second hydride is once again formed as a terminal hydride at Fe6, leading to a mixed dihydride at the cluster (Fig. 5a). Note that the inward-facing Gln176 provides a cavity above Fe6 that still leaves room for a t-hydride. Alternatively, the t-hydride might migrate to the Fe2–Fe6 edge to form a $Fe_2(μ\text{-}H)_2$ core that may allow for straightforward elimination of H_2 (Fig. 5b)[32]. Both conformations are in line with recent spectroscopic data and calculations[66], and a range of available model compounds highlight that the diamond core structure not only is stable (Fig. 5c), but can also support stable N_2 adducts (Fig. 5d)[67–69].

A series of recent theoretical treatments of the role of hydride formation for substrate binding to the cofactors has supported the outstanding role of the Fe2–Fe6 edge of the cofactor[66,70], but they were ambiguous regarding the release of S2B[71]. Complexes with CO for the MoFe protein[43,51] and with CO or a light atom ligand for the VFe protein[33,49,50] consistently showed the full displacement of S2B. The release of S2B is a crucial prerequisite for reorientation of the glutamine residue that blocks proton transfer from the histidine above Fe2 in the hydride accumulation stage. This arrangement is sterically precluded within the tight cofactor binding pocket unless S2B fully dissociates from the metal cluster[33]. Quantum mechanics/molecular mechanics calculations of a reaction pathway of the MoFe protein that includes S2B dissociation indeed reproduce these steps with high accuracy[70].

Among the most striking features of Fe-nitrogenase is that it retains its reactivity towards inert N_2 without the elaborate replacement of an apical iron of the L-cluster with the heterometals Mo or V. The FeFe cofactor appears symmetric, but ligation of the core cluster introduces an important symmetry break via the bidentate homocitrate. Of the two apical iron ions, Fe1 binds to $Cys257^D$, creating a tetrahedral environment like that of Fe2–Fe7. In contrast, Fe8 not only has a non-sulfur protein ligand, $His423^D$, but also two coordinating oxygens from homocitrate, completing an octahedral ligand field. Electronically, these geometries differ substantially, with a stable tetrahedral coordination by weak-field ligands for Fe1 that mandates a high-spin state, but an octahedral geometry with mixed ligands at Fe8 that may afford low- or high-spin states, but also intermediate configurations. The electronic coupling between the iron ions and the distribution of electrons in the different catalytic states influences the total spin of the cluster and thus its reactivity. For the ground state (E_0) of the FeMo cofactor and FeV cofactor, this electron distribution has been analysed by theory and experiment and has highlighted the importance of an antiferromagnetic coupling of Fe2 and Fe6[72]. Based on spatially resolved anomalous dispersion analysis, we have argued that Fe2 and Fe6 are the most oxidized sites in the ground state and thus the likely sites of reduction from the P-cluster[73]. Given that the mechanistic pathways for N_2 reduction are analogous in all isoforms of nitrogenase[34], these two features are expected to be conserved in the FeV and FeFe cofactors. By modulating an apical iron through a different coordination environment, nature thus at least partly replicated the effect of the heterometals Mo or V with the abundant element Fe,

https://doi.org/10.1038/s41929-023-00952-1

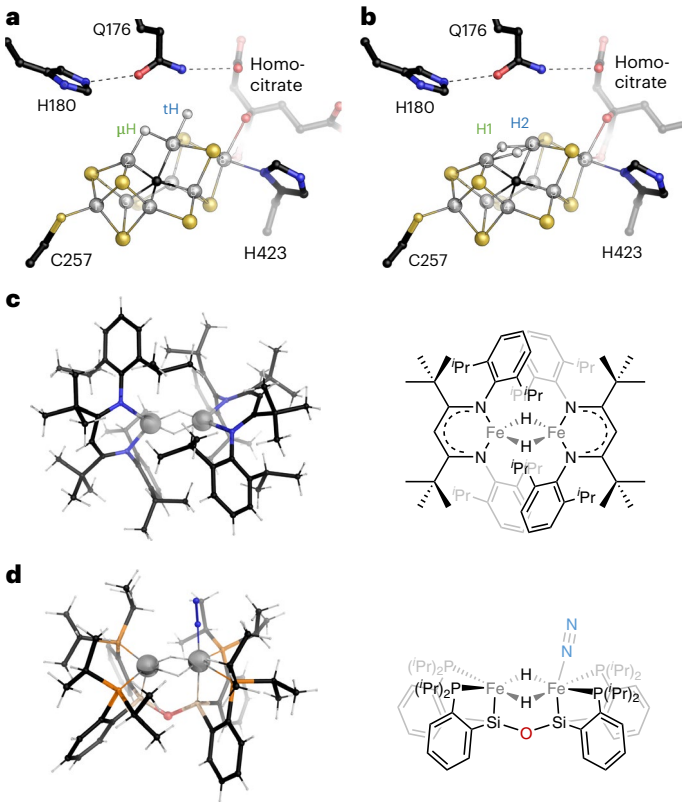

Fig. 5 | Possible E_4 state structures and relevant model complexes. a, Two hydrides occupying the μ-site (μH) and the t-site at Fe6 (tH). With sulfide S2B in the holding site (not shown), Q176 forms a short hydrogen bond to His180, preventing proton transfer to the hydride. **b**, Alternative positioning of two bridging hydrides as a $(Fe–H)_2$ diamond core at the Fe2–Fe6 edge of the cofactor. **c**, The $Fe_2(\mu\text{-}H)_2$ diketiminate complex by Holland and others shows a stable diamond-core structure similar to **b**[75]. **d**, In a $(Fe_2(\mu\text{-}H)_2–N_2)[SiP_2O]$ complex by Rittle and Peters, reduction of the $Fe_2(\mu\text{-}H)_2$ core to a mixed-valent Fe(II)–Fe(I) state led to efficient end-on binding of one or two N_2 molecules[69].

so the octahedral Fe8 probably serves a similar purpose as Mo^{3+} or V^{3+} in the other isoforms.

The structure and properties of Fe-nitrogenase can outline new approaches towards dinitrogen reduction catalysts. In particular, the in situ formation of a super-reduced form of the cofactor by reductive elimination of H_2 from the E_4 state of the catalytic cycle opens an avenue towards N_2 reduction catalysis in an aqueous environment. For this, the key requirements are a dinuclear metal site that allows for terminal or bridging coordination of ligands or substrates, the antiferromagnetic coupling of the metals that favours bridging hydrides, control of proton access to limit hydride loss while charging the cluster towards E_4, and a rigid cluster core that promotes the elimination of H_2 from E_4 rather than stabilizing two bridging hydrides in a relaxed, equatorial geometry[50]. The relevance of reduced, low-coordinate transition-metal complexes for the activation of various substrates has been noted[74], and the ubiquity of metal hydrides in these complexes has led Holland and others to produce a dinuclear $Fe_2(\mu\text{-}H)_2$ complex with bulky β-diketiminate ligands that was capable of N_2 activation (Fig. 5c)[75]. In 2014, a diiron complex $(Fe_2(\mu\text{-}H)_2–N_2)[SiP_2O]$ reported by Rittle and Peters already fulfilled almost all of the above prerequisites, and even bound N_2 terminally upon reduction, albeit without mediating its activation (Fig. 5d)[69]. The analogy of such models to the cofactors of the nitrogenases may be closer than anticipated at the time and might indeed pave a route towards novel, artificial mimics of biological nitrogen fixation.

Methods

Growth of *A. vinelandii* with Mo- and V-depletion

The production and isolation of unmodified iron-only nitrogenase AnfDKG was performed as described elsewhere[24]. In short, *A. vinelandii* Lipman1903[76] cells were deprived of molybdenum by cultivation in modified Burk medium under Mo- and NH_4^+-limiting conditions[77]. Cells were singled out on Burk agar plates that were depleted of molybdenum and any source of fixed nitrogen to select for diazotrophically growing bacteria. Brownish colonies were used to re-inoculate liquid growth medium. After five cycles of incubation in liquid medium followed by selection on agar plates, the cells were exclusively using the iron-only nitrogenase system. Cell growth was performed, by inoculating 100 ml of Mo-free Burk medium with a single colony, followed by incubation for 40 h at 37 °C. Pre-cultures were used to inoculate nitrogen-free 500-ml main cultures followed by overnight incubation at 30 °C. Cells were collected by centrifugation when an optical density at 600 nm of 1.5–2.0 was reached.

Isolation of FeFe protein

The high sensitivity of FeFe protein towards oxygen required all steps to be conducted either in an anerobic chamber (Coy Laboratories) under a 95% N_2/5% H_2 atmosphere or using modified Schlenk techniques under constant supply of pure nitrogen gas. The cell pellet was resuspended in a lysis buffer (50 mM Tris/HCl at pH 7.4, 2.5 mM $Na_2S_2O_4$) and opened at 15,000 psi in an Emulsiflex C-5 homogenizer (Avestin) under N_2 atmosphere. The crude cell extract was then cleared by centrifugation for 1 h at 100,000*g* and the supernatant was then loaded onto a Q Sepharose column (GE Healthcare), equilibrated in lysis buffer. The column was developed with a linear gradient of NaCl, and FeFe protein eluted at 340 mM NaCl. After dilution to 100 mM NaCl, the eluate was loaded onto a second anion exchanger (Resource Q, FE Healthcare), from where it eluted at 200 mM NaCl applied as a linear gradient. Following concentration by ultrafiltration (Vivaspin 20, 100-kDa MWCO, Sartorius) AnfDKG was subjected to a concluding size exclusion chromatography (Superdex S200, GE Healthcare) equilibrated with 20 mM Tris/HCl at pH 7.4, 100 mM NaCl and 2.5 mM $Na_2S_2O_4$ (Extended Data Fig. 1). Pure, concentrated aliquots of 35 mg ml^{-1} were flash-frozen and stored in liquid nitrogen until further use.

Crystallization and data collection

The crystallization of Fe-only nitrogenase from *A. vinelandii* was carried out using the sitting-drop vapour diffusion method under strict exclusion of dioxygen in an anaerobic chamber containing an atmosphere of 95% N_2 and 5% H_2. Crystallization experiments were carried out in 96-well crystallization plates (Swissci 96-well two-drop plate, Hampton Research). A 0.7-μl volume of protein solution containing 10 mg ml^{-1} AnfDKG was mixed with the same volume of a reservoir solution containing 0.1 M Bis-Tris propane/HCl at pH 8.5, 18% (wt/vol) of polyethylene glycol 4000 and 18% (vol/vol) of ethylene glycol. Three-dimensional crystals of Fe-only nitrogenase appeared within four days and, after a week, were collected with a nylon loop then flash-frozen in liquid nitrogen. Diffraction data were collected at the Swiss Light Source (Paul Scherrer Institute) on beamline X06DA using a Pilatus 2 M-F detector at an X-ray wavelength of 1.0000 Å.

Structure solution and refinement

The crystallographic phase problem was solved by molecular replacement, first with the structure of resting-state *A. vinelandii* VFe protein (PDB 5N6Y) as a search model, and subsequently with a homology model generated with AlphaFold2[78]. In both cases, a single predominant solution was obtained using MOLREP[79], and the AlphaFold2 model was then used for iterative rounds of model building and refinement with COOT[80] and REFMAC5[81]. At 1.55 Å spherical resolution, the electron density maps showed clear features for a reduced P-cluster with the same composition and geometry as in other known nitrogenases, and

Table 1 | Data collection and refinement statistics

Data collection	
Space group	$P\,2_12_12_1$
Cell dimensions	
a, *b*, *c* (Å)	110.0, 151.0, 158.9
α, *β*, *γ* (°)	90.0, 90.0, 90.0
Wavelength (Å)	1.0000
Spherical resolution	20.00–1.55
	(1.70–1.55)
Limiting resolution (Å) along	
*a**	1.547 Å
*b**	2.517 Å
*c**	2.204 Å
No. of observations	2,038,399 (92,005)
Unique observations	153,829 (7,691)
R_{merge} [a]	0.109 (1.285)
$R_{p.i.m}$ [b]	0.031 (0.387)
Mean $I/\sigma(I)$	14.9 (2.1)
$CC_{1/2}$ [c]	0.999 (0.662)
Completeness, spherical (%)	40.2 (5.2)
Completeness, ellipsoidal (%)	91.8 (70.4)
B factor from Wilson scaling (Å^2)	21.98
Multiplicity	13.3 (12.0)
Refinement	
Resolution (Å)	20.00–1.55
R_{work} [d] / R_{free} [e]	0.163 / 0.205
No. atoms	
Protein	18,837
Ligand/ion	98
Solvent molecules	1,361
B factors (Å^2)	
Protein	29.85
Ligand/ion	18.63
Water	32.89
Ramachandran plot	
Favoured (%)	96.64
Allowed (%)	2.99
Outliers (%)	0.37
r.m.s deviations	
Bond lengths (Å)	0.007
Bond angles (°)	1.337

Values in parentheses represent the highest-resolution shells. [a]$R_{merge} = \Sigma_{hkl}\Sigma_i|I_i - \langle I\rangle|/\Sigma_{hkl}\Sigma I_i$, where I_i is the intensity of the *i*th observation, is the mean intensity of the reflection and the summations extend over all unique reflections (*hkl*) and all equivalents(*i*), respectively. [b]$R_{pim} = \Sigma_{hkl}[n/(n-1)]^{1/2}\Sigma_i|I_i(hkl) - \langle I(hkl)\rangle|/\Sigma_{hkl}\Sigma_i I_i(hkl)$, where *n* is the multiplicity, and other variables are as defined for R[82]. [c]$CC_{1/2}$ = Pearson correlation coefficient between random half-datasets[83]. [d]$R_{work} = \Sigma_{hkl}||F_{obs}(hkl)| - |F_{calc}(hkl)||/\Sigma_{hkl}|F_{obs}(hkl)||$, where $|F_{obs}|$ and $|F_{calc}|$ are the observed and calculated structure-factor amplitudes, respectively. [e]R_{free} is the cross-validation *R* value for a test set of 5% of unique reflections; here, 7,578 reflections were flagged.

also for the hitherto unknown FeFe cofactor, the catalytic site. Note that, contrary to the atomic-resolution structures of MoFe protein (PDB 3U7Q) and VFe protein (PDB 6FEA, 7ADR, 7ADY and 7AIZ), the present analysis still required the use of geometric restraints for the structure of FeFe cofactor. Restraints were generated from a model of the FeMo cofactor after replacement of Mo for Fe and single-point geometry optimization. Water molecules and ligands were built in additional rounds of refinement and, after translation/libration/screw and restrained refinement with all hydrogens generated by REFMAC5, the final structure had $R_{work} = 0.163$ and $R_{free} = 0.205$ (Table 1). The structure of the heterohexamer as predicted by AlphaFold2.1.1 aligned to the refined model with an r.m.s.d. for all atoms of 1.2 Å, with major differences limited largely to the immediate environment of the metal clusters. Figures were generated with PyMol (Schrödinger).

Reporting summary

Further information on research design is available in the Nature Portfolio Reporting Summary linked to this article.

Data availability

The atomic coordinates and structure factors for *A. vinelandii* Fe-only nitrogenase FeFe protein have been deposited with the Protein Data Bank at http://www.pdb.org with accession code 8BOQ. All other data are available from the authors upon reasonable request. Source data are provided with this paper.

References

1. Canfield, D. E., Glazer, A. N. & Falkowski, P. G. The evolution and future of Earth's nitrogen cycle. *Science* **330**, 192–196 (2010).
2. Rees, D. C. Dinitrogen reduction by nitrogenase—if N_2 isn't broken, it can't be fixed. *Curr. Opin. Struct. Biol.* **3**, 921–928 (1993).
3. Wilson, P. W. & Burris, R. H. The mechanism of biological nitrogen fixation. *Bacteriol. Rev.* **11**, 41–73 (1947).
4. Smil, V. The world's greatest fix: a history of nitrogen in agriculture. *Nature* **431**, 909–910 (2004).
5. Norskov, J. K. & Chen, J. *Sustainable Ammonia Synthesis*, Round Table Report (US DoE, 2016).
6. Chen, J. G. et al. Beyond fossil fuel-driven nitrogen transformations. *Science* **360**, eaar6611 (2018).
7. Ribbe, M. W., Hu, Y. L., Hodgson, K. O. & Hedman, B. Biosynthesis of nitrogenase metalloclusters. *Chem. Rev.* **114**, 4063–4080 (2014).
8. Jimenez-Vicente, E. et al. Sequential and differential interaction of assembly factors during nitrogenase MoFe protein maturation. *J. Biol. Chem.* **293**, 9812–9823 (2018).
9. Einsle, O. & Rees, D. C. Structural enzymology of nitrogenase enzymes. *Chem. Rev.* **120**, 4969–5004 (2020).
10. Bulen, W. A. & LeComte, J. R. Nitrogenase system from *Azotobacter*: 2-enzyme requirement for N_2 reduction, ATP-dependent H_2 evolution and ATP hydrolysis. *Proc. Natl Acad. Sci. USA* **56**, 979–986 (1966).
11. Einsle, O. Nitrogenase FeMo cofactor: an atomic structure in three simple steps. *J. Biol. Inorg. Chem.* **19**, 737–745 (2014).
12. Einsle, O. et al. Nitrogenase MoFe-protein at 1.16 Å resolution: a central ligand in the FeMo-cofactor. *Science* **297**, 1696–1700 (2002).
13. Spatzal, T. et al. Evidence for interstitial carbon in nitrogenase FeMo cofactor. *Science* **334**, 940 (2011).
14. Lancaster, K. M. et al. X-ray emission spectroscopy evidences a central carbon in the nitrogenase iron-molybdenum cofactor. *Science* **334**, 974–977 (2011).
15. Sippel, D. & Einsle, O. The structure of vanadium nitrogenase reveals an unusual bridging ligand. *Nat. Chem. Biol.* **13**, 956–960 (2017).
16. Yang, J. G., Xie, X. Q., Wang, X., Dixon, R. & Wang, Y. P. Reconstruction and minimal gene requirements for the alternative iron-only nitrogenase in *Escherichia coli*. *Proc. Natl Acad. Sci. USA* **111**, E3718–E3725 (2014).
17. Good, A. Toward nitrogen-fixing plants. *Science* **359**, 869–870 (2018).

18. Curatti, L. & Rubio, L. M. Challenges to develop nitrogen-fixing cereals by direct *nif*-gene transfer. *Plant Sci.* **225**, 130–137 (2014).
19. Lee, C. C., Hu, Y. L. & Ribbe, M. W. Vanadium nitrogenase reduces CO. *Science* **329**, 642 (2010).
20. Zheng, Y. N. et al. A pathway for biological methane production using bacterial iron-only nitrogenase. *Nat. Microbiol.* **3**, 281–286 (2018).
21. Diederichs, K. et al. Crystal structure of MalK, the ATPase subunit of the trehalose/maltose ABC transporter of the archaeon *Thermococcus litoralis*. *EMBO J.* **19**, 5951–5961 (2000).
22. Oehlmann, N. N. & Rebelein, J. G. The conversion of carbon monoxide and carbon dioxide by nitrogenases. *ChemBioChem* **23**, e202100453 (2022).
23. Sippel, D. et al. Production and isolation of vanadium nitrogenase from *Azotobacter vinelandii* by molybdenum depletion. *J. Biol. Inorg. Chem.* **22**, 161–168 (2017).
24. Trncik, C., Müller, T., Franke, P. & Einsle, O. Structural analysis of the reductase component AnfH of iron-only nitrogenase from *Azotobacter vinelandii*. *J. Inorg. Biochem.* **227**, 111690 (2022).
25. Dos Santos, P. C. Molecular biology and genetic engineering in nitrogen fixation. *Methods Mol. Biol.* **766**, 81–92 (2011).
26. Chatterjee, R., Ludden, P. W. & Shah, V. K. Characterization of VnfG, the delta subunit of the *vnf*-encoded apodinitrogenase from *Azotobacter vinelandii*—implications for its role in the formation of functional dinitrogenase 2. *J. Biol. Chem.* **272**, 3758–3765 (1997).
27. Danyal, K., Dean, D. R., Hoffman, B. M. & Seefeldt, L. C. Electron transfer within nitrogenase: evidence for a deficit-spending mechanism. *Biochemistry* **50**, 9255–9263 (2011).
28. Duval, S. et al. Electron transfer precedes ATP hydrolysis during nitrogenase catalysis. *Proc. Natl Acad. Sci. USA* **110**, 16414–16419 (2013).
29. Davydov, R. et al. Exploring electron/proton transfer and conformational changes in the nitrogenase MoFe protein and FeMo-cofactor through cryoreduction/EPR measurements. *Isr. J. Chem.* **56**, 841–851 (2016).
30. Decamps, L., Rice, D. B. & DeBeer, S. An Fe_6C Core in all nitrogenase cofactors. *Angew. Chem. Int. Ed.* **61**, e202209190 (2022).
31. Lukoyanov, D. A. et al. ^{13}C-ENDOR characterization of the central carbon within the nitrogenase catalytic cofactor indicates that the CFe_6 core is a stabilizing 'Heart of Steel'. *J. Am. Chem. Soc.* **144**, 18315–18328 (2022).
32. Rohde, M., Sippel, D., Trncik, C., Andrade, S. L. A. & Einsle, O. The critical E_4 state of nitrogenase catalysis. *Biochemistry* **57**, 5497–5504 (2018).
33. Sippel, D. et al. A bound reaction intermediate sheds light on the mechanism of nitrogenase. *Science* **359**, 1484–1489 (2018).
34. Harris, D. F. et al. Mo-, V- and Fe-nitrogenases use a universal eight-electron reductive-elimination mechanism to achieve N_2 reduction. *Biochemistry* **58**, 3293–3301 (2019).
35. Peters, J. W., Fisher, K., Newton, W. E. & Dean, D. R. Involvement of the P-cluster in intramolecular electron-transfer within the nitrogenase MoFe protein. *J. Biol. Chem.* **270**, 27007–27013 (1995).
36. Danyal, K. et al. Uncoupling nitrogenase: catalytic reduction of hydrazine to ammonia by a MoFe protein in the absence of Fe protein-ATP. *J. Am. Chem. Soc.* **132**, 13197–13199 (2010).
37. Zhang, L. M., Morrison, C. N., Kaiser, J. T. & Rees, D. C. Nitrogenase MoFe protein from *Clostridium pasteurianum* at 1.08 Å resolution: comparison with the *Azotobacter vinelandii* MoFe protein. *Acta Crystallogr. D* **71**, 274–282 (2015).
38. Mayer, S. M., Lawson, D. M., Gormal, C. A., Roe, S. M. & Smith, B. E. New insights into structure-function relationships in nitrogenase: a 1.6 Å resolution X-ray crystallographic study of *Klebsiella pneumoniae* MoFe-protein. *J. Mol. Biol.* **292**, 871–891 (1999).
39. Owens, C. P., Katz, F. E. H., Carter, C. H., Oswald, V. F. & Tezcan, F. A. Tyrosine-coordinated P-cluster in *G. diazotrophicus* nitrogenase: evidence for the importance of O-based ligands in conformationally gated electron transfer. *J. Am. Chem. Soc.* **138**, 10124–10127 (2016).
40. Zheng, L. M., White, R. H. & Dean, D. R. Purification of the *Azotobacter vinelandii nifV*-encoded homocitrate synthase. *J. Bacteriol.* **179**, 5963–5966 (1997).
41. Kennedy, C. & Dean, D. The NifU, NifS and NifV gene-products are required for activity of all 3 nitrogenases of *Azotobacter vinelandii*. *Mol. Gen. Genet.* **231**, 494–498 (1992).
42. Hwang, J. C., Chen, C. H. & Burris, R. H. Inhibition of nitrogenase-catalyzed reductions. *Biochim. Biophys. Acta* **292**, 256–270 (1973).
43. Spatzal, T., Perez, K. A., Einsle, O., Howard, J. B. & Rees, D. C. Ligand binding to the FeMo-cofactor: structures of CO-bound and reactivated nitrogenase. *Science* **345**, 1620–1623 (2014).
44. Spatzal, T., Perez, K. A., Howard, J. B. & Rees, D. C. Catalysis-dependent selenium incorporation and migration in the nitrogenase active site iron-molybdenum cofactor. *eLife* **4**, e11620 (2015).
45. Thorneley, R. N. F. & Lowe, D. J. in *Molybdenum Enzymes 1* (ed. Spiro, T. G.) 221–284 (Wiley, 1985).
46. Lukoyanov, D. et al. Reductive elimination of H_2 activates nitrogenase to reduce the N-N triple bond: characterization of the E_4(4H) Janus intermediate in wild-type enzyme. *J. Am. Chem. Soc.* **138**, 10674–10683 (2016).
47. Lukoyanov, D. et al. Unification of reaction pathway and kinetic scheme for N_2 reduction catalyzed by nitrogenase. *Proc. Natl Acad. Sci. USA* **109**, 5583–5587 (2012).
48. Lukoyanov, D. et al. Identification of a key catalytic intermediate demonstrates that nitrogenase is activated by the reversible exchange of N_2 for H_2. *J. Am. Chem. Soc.* **137**, 3610–3615 (2015).
49. Rohde, M., Grunau, K. & Einsle, O. CO binding to the FeV cofactor of CO-reducing vanadium nitrogenase at atomic resolution. *Angew. Chem. Int. Ed.* **59**, 23626–23630 (2020).
50. Rohde, M., Laun, K., Zebger, I., Stripp, S. T. & Einsle, O. Two ligand-binding sites in CO-reducing V nitrogenase reveal a general mechanistic principle. *Sci. Adv.* **7**, eabg4474 (2021).
51. Buscagan, T. M., Perez, K. A., Maggiolo, A. O., Rees, D. C. & Spatzal, T. Structural characterization of two CO molecules bound to the nitrogenase active site. *Angew. Chem. Int. Ed.* **60**, 5704–5707 (2021).
52. Kang, W., Lee, C. C., Jasniewski, A. J., Ribbe, M. W. & Hu, Y. Structural evidence for a dynamic metallocofactor during N_2 reduction by Mo-nitrogenase. *Science* **368**, 1381–1385 (2020).
53. Bergmann, J., Oksanen, E. & Ryde, U. Critical evaluation of a crystal structure of nitrogenase with bound N_2 ligands. *J. Biol. Inorg. Chem.* **26**, 341–353 (2021).
54. Peters, J. W. et al. Comment on 'Structural evidence for a dynamic metallocofactor during N_2 reduction by Mo-nitrogenase'. *Science* **371**, eabe5481 (2021).
55. Lee, C. C. et al. Evidence of substrate binding and product release via belt-sulfur mobilization of the nitrogenase cofactor. *Nat. Catal.* **5**, 443–454 (2022).
56. Eady, R. R. Structure-function relationships of alternative nitrogenases. *Chem. Rev.* **96**, 3013–3030 (1996).
57. Garcia, A. K., Kolaczkowski, B. & Kaçar, B. Reconstruction of nitrogenase predecessors suggests origin from maturase-like proteins. *Genome Biol. Evol.* **14**, evac031 (2022).
58. Perez-Gonzalez, A. et al. Specificity of NifEN and VnfEN for the assembly of nitrogenase active site cofactors in *Azotobacter vinelandii*. *mBio* **12**, e0156821 (2021).

59. Liang, J. H., Madden, M., Shah, V. K. & Burris, R. H. Citrate substitutes for homocitrate in nitrogenase of a *nifV* mutant of *Klebsiella pneumoniae*. *Biochemistry* **29**, 8577–8581 (1990).
60. Mayer, S. M., Gormal, C. A., Smith, B. E. & Lawson, D. M. Crystallographic analysis of the MoFe protein of nitrogenase from a *nifV* mutant of *Klebsiella pneumoniae* identifies citrate as a ligand to the molybdenum of iron molybdenum cofactor (FeMoco). *J. Biol. Chem.* **277**, 35263–35266 (2002).
61. Cao, L. L., Caldararu, O. & Ryde, U. Protonation states of homocitrate and nearby residues in nitrogenase studied by computational methods and quantum refinement. *J. Phys. Chem. B* **121**, 8242–8262 (2017).
62. Nicolet, Y. et al. Crystallographic and FTIR spectroscopic evidence of changes in Fe coordination upon reduction of the active site of the Fe-only hydrogenase from *Desulfovibrio desulfuricans*. *J. Am. Chem. Soc.* **123**, 1596–1601 (2001).
63. Fontecilla-Camps, J. C., Volbeda, A., Cavazza, C. & Nicolet, Y. Structure/function relationships of [NiFe]- and [FeFe]-hydrogenases. *Chem. Rev.* **107**, 4273–4303 (2007).
64. Van Stappen, C. et al. Spectroscopic description of the E_1 state of Mo nitrogenase based on Mo and Fe X-ray absorption and Mössbauer studies. *Inorg. Chem.* **58**, 12365–12376 (2019).
65. Van Stappen, C., Thorhallsson, A. T., Decamps, L., Björnsson, R. & DeBeer, S. Resolving the structure of the E_1 state of Mo nitrogenase through Mo and Fe K-edge EXAFS and QM/MM calculations. *Chem. Sci.* **10**, 9807–9821 (2019).
66. Lukoyanov, D. A. et al. Electron redistribution within the nitrogenase active site FeMo-cofactor during reductive elimination of H2 to achieve N≡N triple-bond activation. *J. Am. Chem. Soc.* **142**, 21679–21690 (2020).
67. Yu, Y. et al. The reactivity patterns of low-coordinate iron-hydride complexes. *J. Am. Chem. Soc.* **130**, 6624–6638 (2008).
68. Coric, I. & Holland, P. L. Insight into the iron molybdenum cofactor of nitrogenase from synthetic iron complexes with sulfur, carbon and hydride ligands. *J. Am. Chem. Soc.* **138**, 7200–7211 (2016).
69. Rittle, J., McCrory, C. C. L. & Peters, J. C. A 10^6-fold enhancement in N_2-binding affinity of an $Fe_2(\mu\text{-}H)_2$ core upon reduction to a mixed-valence $Fe^{II}Fe^{I}$ state. *J. Am. Chem. Soc.* **136**, 13853–13862 (2014).
70. Cao, L. L. & Ryde, U. Putative reaction mechanism of nitrogenase after dissociation of a sulfide ligand. *J. Catal.* **391**, 247–259 (2020).
71. Thorhallsson, A. T. & Björnsson, R. The E_2 state of FeMoco: hydride formation versus Fe reduction and a mechanism for H_2 evolution. *Chem. Eur. J.* **27**, 16788–16800 (2021).
72. Rees, J. A. et al. Comparative electronic structures of nitrogenase FeMoco and FeVco. *Dalton Trans.* **46**, 2445–2455 (2017).
73. Spatzal, T. et al. Nitrogenase FeMoco investigated by spatially resolved anomalous dispersion refinement. *Nat. Commun.* **7**, 10902 (2016).
74. Cummins, C. C. Three-coordinate complexes of 'Hard' ligands: advances in synthesis, structure and reactivity. *Prog. Inorg. Chem.* **47**, 685–836 (1998).
75. Smith, J. M., Lachicotte, R. J. & Holland, P. L. N=N bond cleavage by a low-coordinate iron(II) hydride complex. *J. Am. Chem. Soc.* **125**, 15752–15753 (2003).
76. Lipman, J. G. Experiments on the transformation and fixation of nitrogen by bacteria. *Rep. N. Jersey Agric. Exp. Stat.* **24**, 217–285 (1903).
77. Subba Rao, N. S. *Soil Microorganisms and Plant Growth* 3rd edn (Science, 1995).
78. Jumper, J. et al. Highly accurate protein structure prediction with AlphaFold. *Nature* **596**, 583–589 (2021).
79. Vagin, A. & Teplyakov, A. Molecular replacement with MOLREP. *Acta Crystallogr. D* **66**, 22–25 (2010).
80. Emsley, P., Lohkamp, B., Scott, W. G. & Cowtan, K. Features and development of Coot. *Acta Crystallogr. D* **66**, 486–501 (2010).
81. Murshudov, G. N. et al. REFMAC5 for the refinement of macromolecular crystal structures. *Acta Crystallogr. D* **67**, 355–367 (2011).
82. Weiss, M. & Hilgenfeld, R. On the use of the merging *R* factor as a quality indicator for X-ray data. *J. Appl. Crystallogr.* **30**, 203–205 (1997).
83. Karplus, P. A. & Diederichs, K. Linking crystallographic model and data quality. *Science* **336**, 1030–1033 (2012).
84. Okada, T., Tomita, T., Wulandari, A. P., Kuzuyama, T. & Nishiyama, M. Mechanism of substrate recognition and insight into feedback inhibition of homocitrate synthase from *Thermus thermophilus*. *J. Biol. Chem.* **285**, 4195–4205 (2010).

Acknowledgements

This work was supported by the European Research Council (grant no. 310656) and Deutsche Forschungsgemeinschaft (PP 1927, project ID 311061829, and RTG 1976, project ID 235777276). We thank P. dos Santos, M. Rohde, K. Parison, J. Gies-Elterlein, F. Schneider, S.L.A. Andrade and P. Franke for helpful discussions and the beamline staff at the Swiss Light Source, Villigen, Switzerland, for excellent assistance with data collection.

Author contributions

C.T. and O.E. designed the experiments. C.T. and F.D. produced protein and generated crystals. C.T. and O.E. built and refined the crystal structure. C.T., F.D. and O.E. analysed data and wrote the paper.

Competing interests

The authors declare no competing interests.

Additional information

Extended data is available for this paper at https://doi.org/10.1038/s41929-023-00952-1.

Supplementary information The online version contains supplementary material available at https://doi.org/10.1038/s41929-023-00952-1.

Correspondence and requests for materials should be addressed to Oliver Einsle.

Peer review information *Nature Catalysis* thanks Per Siegbahn, Tristan Wagner and the other, anonymous, reviewer(s) for their contribution to the peer review of this work.

Reprints and permissions information is available at www.nature.com/reprints.

Publisher's note Springer Nature remains neutral with regard to jurisdictional claims in published maps and institutional affiliations.

Springer Nature or its licensor (e.g. a society or other partner) holds exclusive rights to this article under a publishing agreement with the author(s) or other rightsholder(s); author self-archiving of the accepted manuscript version of this article is solely governed by the terms of such publishing agreement and applicable law.

© The Author(s), under exclusive licence to Springer Nature Limited 2023

https://doi.org/10.1038/s41929-023-00952-1

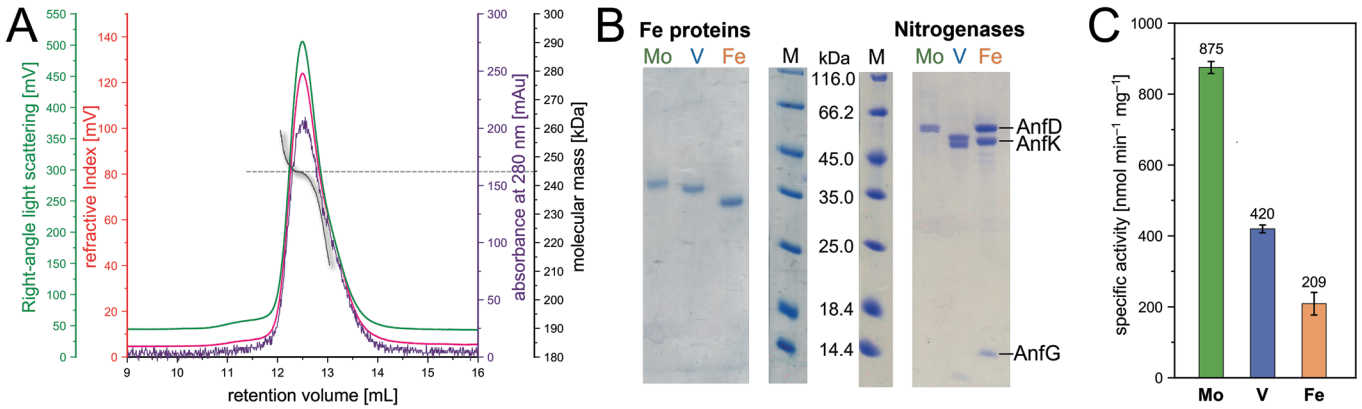

Extended Data Fig. 1 | Isolation and characterization of Fe nitrogenase from *Azotobacter vinelandii*. **a**) Analytical size exclusion chromatography of FeFe protein on Superdex S200 (Cytiva), using a triple detector array with UV absorbance (purple), right-angle light scattering (green) and refractive index (red). The derived absolute molecular mass is shown in black. **b**) SDS-PAGE of preparations of the three Fe proteins of *A. vinelandii* (left) and the three dinitrogenases (right). **c**) N_2 reduction activities of the three *A. vinelandii* nitrogenase isoenzymes with their respective Fe proteins. Data from three technical replicates from the protein batch used for structure determination, presented as mean values +/− standard deviation.

https://doi.org/10.1038/s41929-023-00952-1

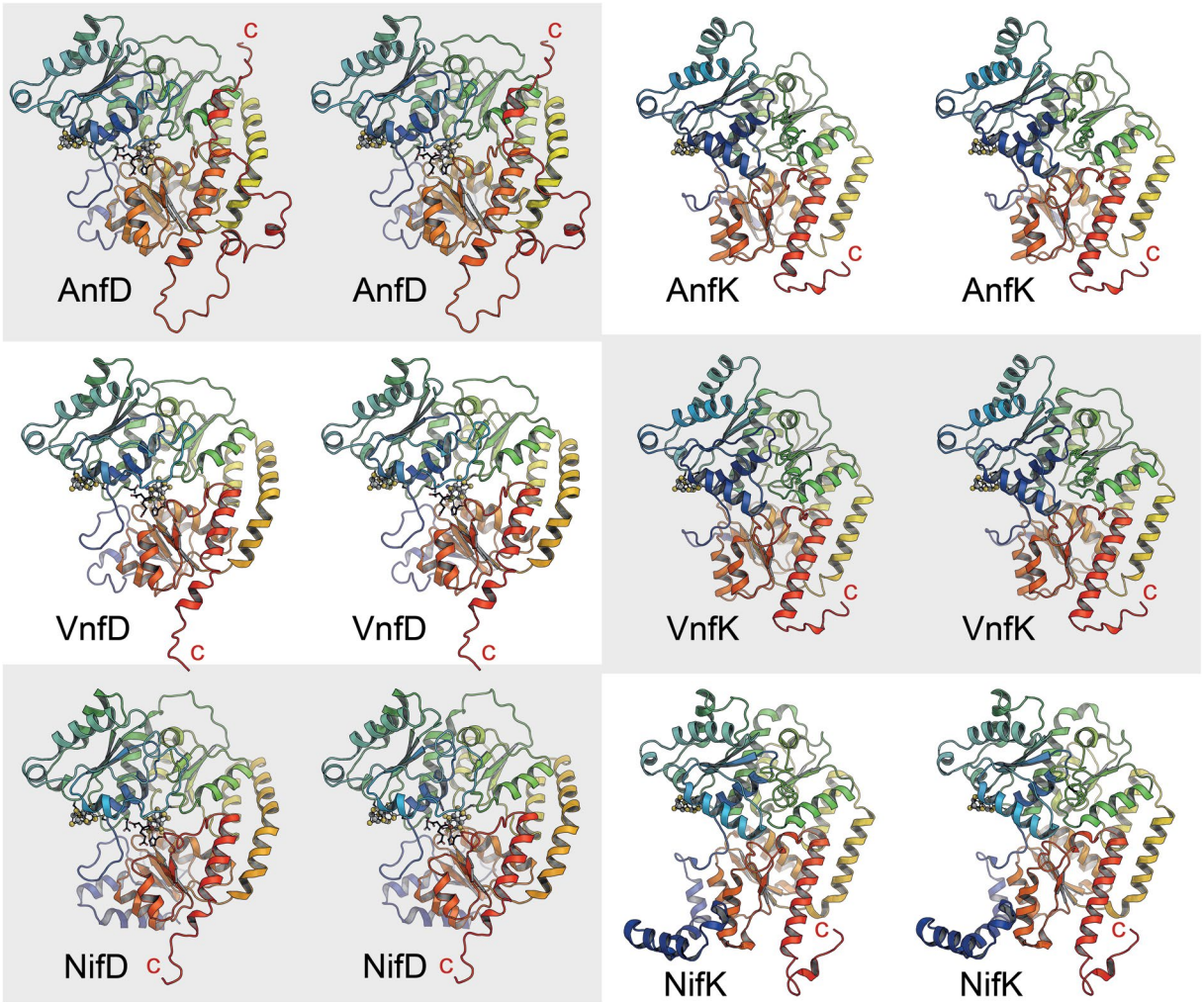

Extended Data Fig. 2 | Structural comparison of the dinitrogenase core subunits of *A. vinelandii*. Stereo images of the D- and K-subunits of Fe-, V-, and Mo-nitrogenases (top to bottom) in identical orientation, colored from blue at the N-terminus to red on the C-terminus. The respective cofactors are shown in the D-subunits, P-clusters are shown in both subunits to emphasize their position in the interface. Note the extended C-terminus of AnfD and N-terminus of NifK that in part occupy the same position within the quaternary structure of the respective dinitrogenases (Fig. 1a, Extended Data Fig. 3).

https://doi.org/10.1038/s41929-023-00952-1

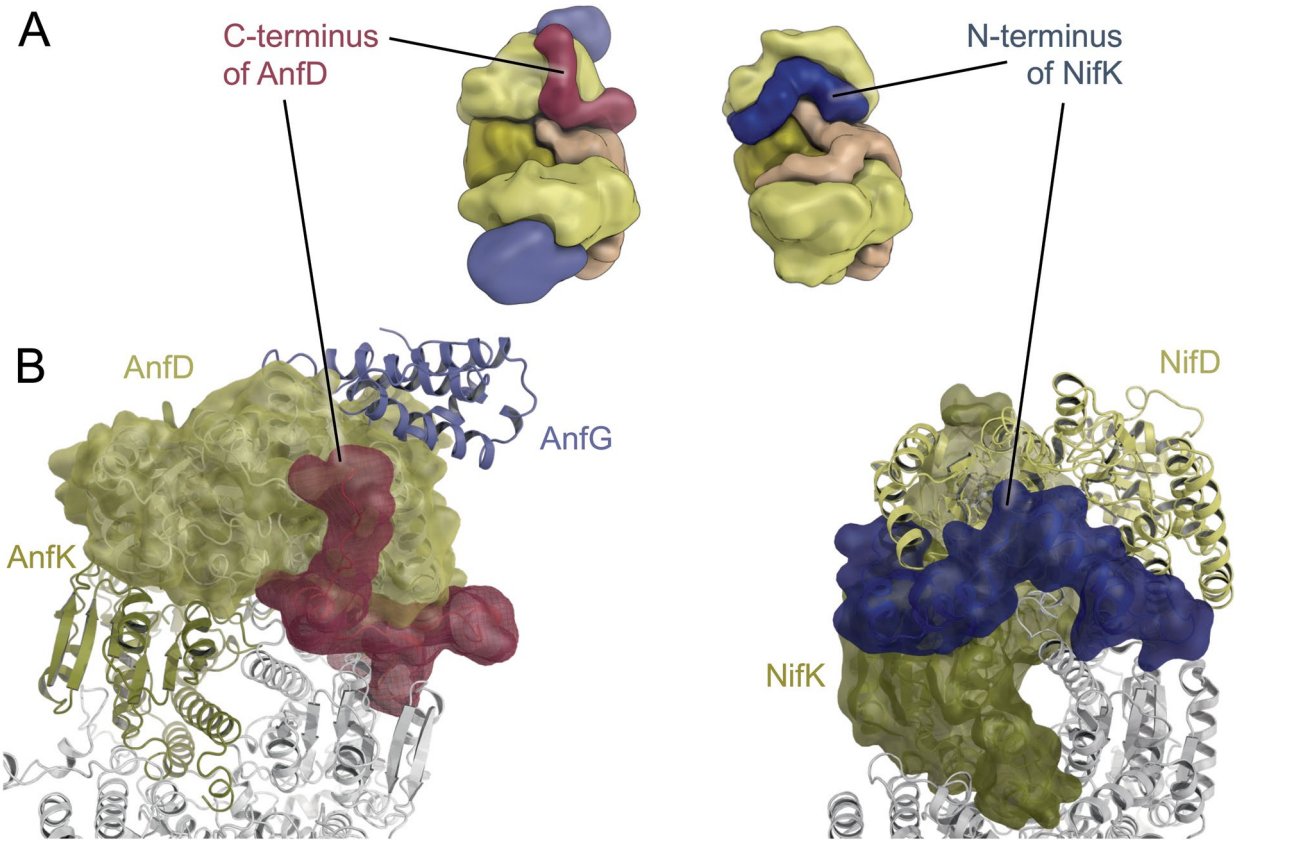

Extended Data Fig. 3 | Structural Differences and Similarities between Mo- and Fe-nitrogenase. a) Schematic representation of Fe-nitrogenase (left) and Mo-nitrogenase (right) from *A. vinelandii*. Although the surfaces of both enzymes appear distinct, the extended C-terminus of AnfD (red) occupies a very similar position on the protein surface as the C-terminus of NifK (blue). **b**) Detail views of A) with surface representations for AnfD with its C-terminus (left) and NifK with its N-terminus.

https://doi.org/10.1038/s41929-023-00952-1

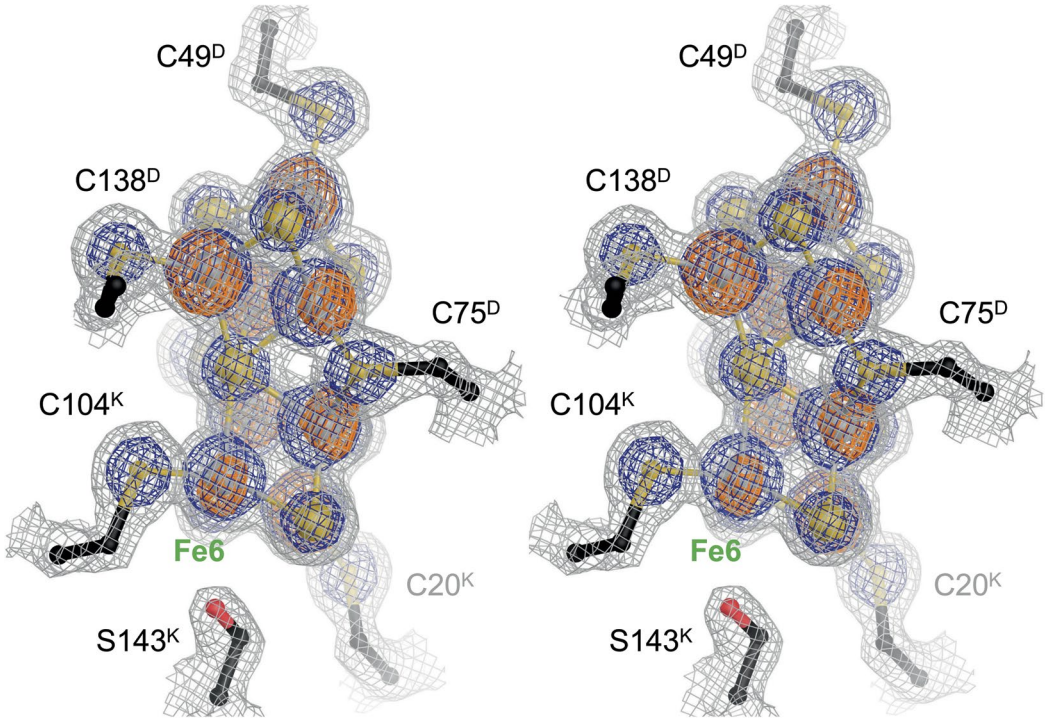

Extended Data Fig. 4 | The P-cluster in *A. vinelandii* Fe nitrogenase. The [8Fe:7S] cluster in the structure is observed in the all-ferrous P^N state. The labelled Fe6 that moves towards the conserved serine $S143^K$ upon oxidation to the P^{+1} state does not show the dual conformation that is frequently observed in crystal structures. The stereo image shows the $2F_o–F_c$ electron density map contoured at the 2σ level (grey) and the 6σ level (blue), as well as an anomalous difference electron density map collected at the Fe K-edge contoured at the 5σ level (orange).

https://doi.org/10.1038/s41929-023-00952-1

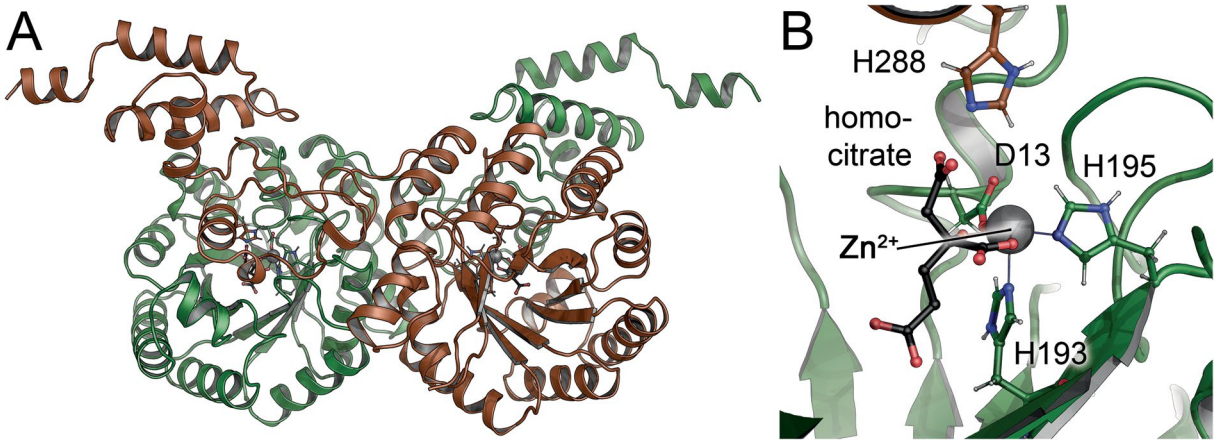

Extended Data Fig. 5 | Homocitrate synthase from *A. vinelandii*. **a**) Structure of the NifV gene product as predicted by Alphafold2. Like other known enzymes of this type, NifV forms a homodimer with a TIM-barrel domain that coordinates a Zn^{2+} ion in its centre as the active site. The metal ion and a homocitrate ligand were modelled based on the structure of *R*-homocitrate synthase from *Thermus thermophilus* (PDB 2ZTK)[84]. Homocitrate is formed by the condensation of 2-oxoglutarate with acetyl-CoA. **b**) The modelled metal site of NifV. Zn^{2+} is coordinated by two histidine and one aspartate residue. During catalysis, 2-oxoglutarate binds as a bidentate ligand to the metal and is then reacted with the acetyl group of acetyl-CoA.

https://doi.org/10.1038/s41929-023-00952-1

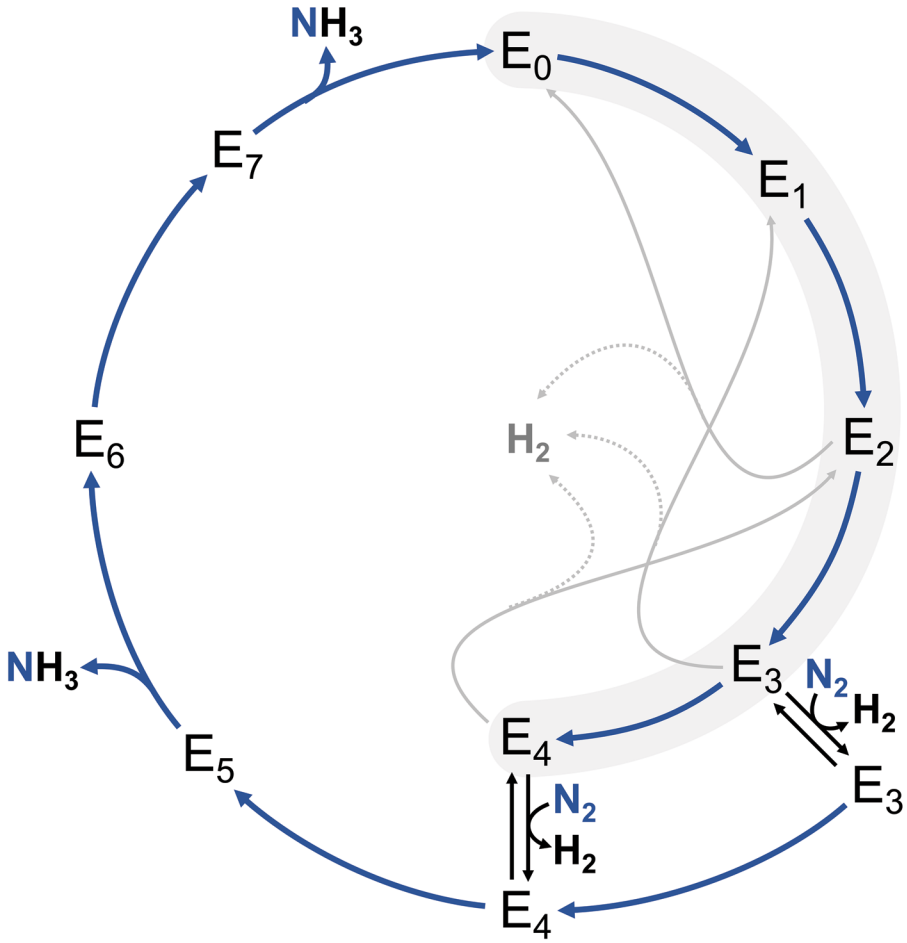

Extended Data Fig. 6 | Kinetic Scheme for N_2 reduction by nitrogenases according to Lowe and Thorneley. Catalysing an eight-electron process, the enzyme cycles through eight states E_0–E_7, in which each electron transfer (blue arrows) is accompanied by a protonation event for charge compensation. In an initial charging phase (grey), the enzyme must be reduced from its resting state E_0 to at least E_3, more likely E_4, to gain the ability to bind and activate N_2. From E_2 on, unproductive H_2 release is observed, which is commonly interpreted as the (unwanted) protonation of a surface hydride on the cofactor, turning the enzyme back two states in the cycle. In contrast, the H_2 released in E_4 is the result of the reductive elimination of H_2 from *two* hydrides, leaving the cofactor in a 2-electron-reduced state that is uniquely capable of N_2 binding and activation. The remaining steps of substrate reduction (E_5–E_7) are then facile. Lowe and Thorneley did not observe H_2 formation from these states, indicating that no further surface hydrides are formed, and reduction occurs directly on the bound intermediates.

nature portfolio

Corresponding author(s): Oliver EINSLE

Last updated by author(s): Nov 15, 2022

Reporting Summary

Nature Portfolio wishes to improve the reproducibility of the work that we publish. This form provides structure for consistency and transparency in reporting. For further information on Nature Portfolio policies, see our Editorial Policies and the Editorial Policy Checklist.

Statistics

For all statistical analyses, confirm that the following items are present in the figure legend, table legend, main text, or Methods section.

n/a	Confirmed
☒	☐ The exact sample size (*n*) for each experimental group/condition, given as a discrete number and unit of measurement
☐	☒ A statement on whether measurements were taken from distinct samples or whether the same sample was measured repeatedly
☒	☐ The statistical test(s) used AND whether they are one- or two-sided *Only common tests should be described solely by name; describe more complex techniques in the Methods section.*
☒	☐ A description of all covariates tested
☒	☐ A description of any assumptions or corrections, such as tests of normality and adjustment for multiple comparisons
☒	☐ A full description of the statistical parameters including central tendency (e.g. means) or other basic estimates (e.g. regression coefficient) AND variation (e.g. standard deviation) or associated estimates of uncertainty (e.g. confidence intervals)
☒	☐ For null hypothesis testing, the test statistic (e.g. *F*, *t*, *r*) with confidence intervals, effect sizes, degrees of freedom and *P* value noted *Give P values as exact values whenever suitable.*
☒	☐ For Bayesian analysis, information on the choice of priors and Markov chain Monte Carlo settings
☒	☐ For hierarchical and complex designs, identification of the appropriate level for tests and full reporting of outcomes
☒	☐ Estimates of effect sizes (e.g. Cohen's *d*, Pearson's *r*), indicating how they were calculated

Our web collection on statistics for biologists contains articles on many of the points above.

Software and code

Policy information about availability of computer code

Data collection	DECTRIS Eiger 16M
Data analysis	XDS, autoProc (Global Phasing Ltd.), Coot, REFMAC5

For manuscripts utilizing custom algorithms or software that are central to the research but not yet described in published literature, software must be made available to editors and reviewers. We strongly encourage code deposition in a community repository (e.g. GitHub). See the Nature Portfolio guidelines for submitting code & software for further information.

Data

Policy information about availability of data

All manuscripts must include a data availability statement. This statement should provide the following information, where applicable:

- Accession codes, unique identifiers, or web links for publicly available datasets
- A description of any restrictions on data availability
- For clinical datasets or third party data, please ensure that the statement adheres to our policy

The structural model and structure factors have been deposited with the Protein Data Bank at www.pdb.org under the accession number 8BOQ.

Human research participants

Policy information about studies involving human research participants and Sex and Gender in Research.

Reporting on sex and gender	N/A
Population characteristics	N/A
Recruitment	N/A
Ethics oversight	N/A

Note that full information on the approval of the study protocol must also be provided in the manuscript.

Field-specific reporting

Please select the one below that is the best fit for your research. If you are not sure, read the appropriate sections before making your selection.

☒ Life sciences ☐ Behavioural & social sciences ☐ Ecological, evolutionary & environmental sciences

For a reference copy of the document with all sections, see nature.com/documents/nr-reporting-summary-flat.pdf

Life sciences study design

All studies must disclose on these points even when the disclosure is negative.

Sample size	The data reported here was collected from a single crystal. Data collection and refinement statistics are summarized in Table S1.
Data exclusions	Diffraction data were excluded according to a CC(1/2) cutoff.
Replication	Production and isolation of FeFe protein of nitrogenase was fully reproducible, as judged by SEC and PAGE. A large number >20 data sets of different crystal were collected and analyzed and were highly consistent. The data set reported here is the one of the highest quality.
Randomization	This study does not include any experiments that require randomized samples.
Blinding	This study does not include any experiments that require blinding.

Reporting for specific materials, systems and methods

We require information from authors about some types of materials, experimental systems and methods used in many studies. Here, indicate whether each material, system or method listed is relevant to your study. If you are not sure if a list item applies to your research, read the appropriate section before selecting a response.

Materials & experimental systems

n/a	Involved in the study
☒	☐ Antibodies
☒	☐ Eukaryotic cell lines
☒	☐ Palaeontology and archaeology
☒	☐ Animals and other organisms
☒	☐ Clinical data
☒	☐ Dual use research of concern

Methods

n/a	Involved in the study
☒	☐ ChIP-seq
☒	☐ Flow cytometry
☒	☐ MRI-based neuroimaging